



## Ru-In/H-SSZ-13 for the selective reduction of nitric oxide by methane: Insights from temperature-programmed desorption studies

Jun Yang<sup>a</sup>, Yupeng Chang<sup>a</sup>, Weili Dai<sup>a</sup>, Guangjun Wu<sup>a</sup>, Naijia Guan<sup>a,b</sup>, Landong Li<sup>a,b,\*</sup>

<sup>a</sup> School of Materials Science and Engineering & National Institute for Advanced Materials, Nankai University, Tianjin, 300350, PR China

<sup>b</sup> Key Laboratory of Advanced Energy Materials Chemistry of the Ministry of Education, Collaborative Innovation Center of Chemical Science and Engineering, PR China



### ARTICLE INFO

#### Keywords:

Selective catalytic reduction  
Nitric oxide  
Methane  
Ru-In/H-SSZ-13  
Temperature-programmed desorption

### ABSTRACT

The selective catalytic reduction of nitric oxide by methane ( $\text{CH}_4$ -SCR) represents the most desirable technique for the post-treatment of nitrogen oxide emissions from gas-fired power plants and the efficient  $\text{CH}_4$ -SCR catalysts are being explored. We herein report the construction of bimetallic Ru-In/H-SSZ-13 catalyst, which exhibited remarkable performance in  $\text{CH}_4$ -SCR under the reaction conditions of a high gas hourly space velocity (GHSV) of 75,000  $\text{h}^{-1}$  and in the presence of 6%  $\text{H}_2\text{O}$ . In Ru-In/H-SSZ-13, the close contact between Ru and In species was confirmed by transmission electron microscopy (TEM) analysis, and their electronic interaction was verified by means of X-ray photoelectron spectroscopy (XPS) and temperature-programmed reduction by hydrogen ( $\text{H}_2$ -TPR). All these features made Ru-In/H-SSZ-13 an elegant example of zeolite-based cooperative catalytic system for  $\text{CH}_4$ -SCR. The surface species formed and their stability on Ru/H-SSZ-13, In/H-SSZ-13 and Ru-In/H-SSZ-13 were investigated by temperature-programmed desorption (TPD) experiments, from which the individual role of H-SSZ-13, Ru and In sites and their cooperation in  $\text{CH}_4$ -SCR were discussed in detail.

### 1. Introduction

Nitrogen oxides ( $\text{NO}_x$ , including NO and  $\text{NO}_2$ ), along with sulfur oxide ( $\text{SO}_2$ ), non-methane volatile organic compounds (NMVOCs) and ammonia ( $\text{NH}_3$ ), are recognized as the major air pollutants that do great harm to the environment and human health [1,2]. The selective catalytic reduction (SCR) technology has been extensively investigated for the post-treatment of  $\text{NO}_x$  in excess oxygen and different types of reductants, e.g.  $\text{NH}_3$  [3–7],  $\text{H}_2$  [8–10], hydrocarbons [11–16] and oxygentanes [17,18], have been employed.  $\text{NH}_3$ -SCR has been commercialized in  $\text{NO}_x$  abatement from coal-fired power plants and heavy-duty diesel engines for years. Under the background of replacing coal by natural gas (main component:  $\text{CH}_4$ ) as clean fuel for urban power plants,  $\text{CH}_4$ -SCR has been receiving more and more attention in recent years [11,19–34]. Compared with  $\text{NH}_3$ ,  $\text{CH}_4$  appears to be a more attractive reductant in gas-fired power plants due to its noncorrosive and easily-available characteristics. On the other hand,  $\text{CH}_4$  is chemical inert and hard to be activated, which makes  $\text{CH}_4$ -SCR more difficult than  $\text{NH}_3$ -SCR. To our knowledge, the efficient  $\text{CH}_4$ -SCR catalysts working under simulated conditions of gas-fired power plant exhaust, i.e. at high gas-hourly space velocities (GHSVs) and in the presence of excess steam, are still being explored.

Zeolites can provide ideal scaffolds for redox active components and

additional acid sites, e.g. Brønsted acid sites, for SCR reaction, making them the most promising support materials for  $\text{deNO}_x$  applications [4,6,12,35–37]. Currently, the small-pore zeolites (e.g. CHA [5,7,38], KFI [39] and LTA [40]) are attracting more attention than the medium-pore (e.g. MFI and FER) or large-pore (e.g. FAU and BEA) zeolites for  $\text{NH}_3$ -SCR. A major advantage of small-pore zeolites lies in their good stability against framework dealumination, which should be more important for  $\text{CH}_4$ -SCR at high reaction temperatures (~500 °C). However, to our knowledge, the small-pore zeolites are rarely employed as support materials for  $\text{CH}_4$ -SCR catalysts. For the  $\text{CH}_4$ -SCR reaction, In-containing zeolites have been extensively investigated during the past decades [23–29]. To improve the catalytic performance of In-containing zeolites, modifications by a second transition metal, e.g. Ce [30], Fe [31], Pd [32], Co [33] and La [34], have been reported to be a feasible strategy. The major role of the second transition metal is proposed to promote the oxidative activation of NO for  $\text{CH}_4$ -SCR.

Inspired by the above-mentioned research progresses, we herein report the design of a robust Ru-In/H-SSZ-13 catalyst for  $\text{CH}_4$ -SCR, which exhibits remarkable catalytic performance under harsh reaction conditions, i.e. at a high GHSV of 75,000  $\text{h}^{-1}$  and in the presence of 6% steam. H-SSZ-13 is employed as zeolite support to ensure the stability of catalyst as well as to create the close interaction between In and Ru species. For an insight into the individual role of Ru, In and H-SSZ-13

\* Corresponding author at: School of Materials Science and Engineering & National Institute for Advanced Materials, Nankai University, Tianjin, 300350, PR China.  
E-mail address: [lild@nankai.edu.cn](mailto:lild@nankai.edu.cn) (L. Li).

during CH<sub>4</sub>-SCR, the stability of surface species formed on Ru-In/H-SSZ-13 (dominating N<sub>x</sub>O<sub>y</sub> species) is investigated by means of temperature-programmed desorption technique, which has been widely employed in studying lean NO<sub>x</sub> traps [41–44].

## 2. Experimental

### 2.1. Catalyst preparation

The chemical reagents were purchased from Alfa Aesar (analytical grade) and used directly as received. All catalysts were prepared by wet impregnation in which various commercial zeolites in their H-forms (from Sinopec), i.e. H-SSZ-13 (Si/Al = 12), H-ZSM-5 (Si/Al = 12), H-beta (Si/Al = 12), H-mordenite (Si/Al = 11) and SAPO-34 (P/Si = 4), were used as supports. In a typical process, desired amounts of metal precursors (see Supporting Information for details) were dissolved in excess water to form solution, to which zeolite support was added. After stirring at room temperature for 24 h, slurry was obtained and the water was removed in a rotary evaporator at 80 °C at reduced pressure. The solid residue was dried, heated in Ar at 550 °C for 2 h, reduced in 10% H<sub>2</sub>/Ar at 450 °C for 1 h and re-oxidized in 10% O<sub>2</sub>/Ar at 450 °C for 1 h. The final product was denoted as x%Me-y%In/Z, where x% and y% indicated the weight loadings of the second metal and In, respectively, and Z represented the type of zeolite support.

### 2.2. Catalyst characterization

The chemical compositions of samples were analyzed on an IRIS Advantage inductively coupled plasma atomic emission spectrometer (ICP-AES).

The X-ray diffraction (XRD) patterns of selected zeolite samples were recorded on a Bruker D8 ADVANCE powder diffractometer with a Cu-K $\alpha$  radiation ( $\lambda = 0.1542$  nm) at a scanning rate of 4°/min in the region of 5–50°.

The transmission electron microscopy (TEM) images of selected zeolite samples were acquired on a FEI Tecnai G<sup>2</sup> F20 electron microscope. The high angle annular dark field scanning transmission electron microscopy (HAADF-STEM) images were acquired on a FEI Talos electron microscope. Element mapping analysis was performed under HAADF-STEM mode using a FEI built-in energy dispersive spectrum.

The X-ray photoelectron spectra (XPS) of samples were conducted on a Thermo Scientific ESCALAB 250Xi spectrometer with monochromatic AlK $\alpha$  X-ray source ( $h\nu = 1486.6$  eV). The accurate binding energies ( $\pm 0.1$  eV) were determined with reference to the C 1 s line of adventitious carbon at 284.8 eV.

The experiments of temperature-programmed reduction by hydrogen (H<sub>2</sub>-TPR) were performed on a Quantachrome ChemBET 3000 chemisorption analyzer. Typically, the sample of ca. 0.1 g was pretreated in flowing Ar at 300 °C, cooled to 50 °C in the same atmosphere and purged with 5%H<sub>2</sub>/Ar for 30 min. H<sub>2</sub>-TPR was then performed in flowing 5%H<sub>2</sub>/Ar (30 mL/min) at a heating rate of 10 °C/min.

The Ar adsorption-desorption isotherms of samples before and after CH<sub>4</sub>-SCR reaction were measured at –186 °C on a Quantachrome iQ-MP gas adsorption analyzer. Before Ar adsorption, the samples were dehydrated at 200 °C for 2 h. The total surface area was calculated via the Brunauer Emmett Teller (BET) equation.

The water uptake experiments at 27 °C were also performed on the Quantachrome iQ-MP gas adsorption analyzer. Before the adsorption measurements, the calcined samples were degassed at 200 °C overnight.

The <sup>27</sup>Al solid-state magic angle spinning nuclear magnetic resonance (MAS NMR) spectra were performed with hydrated samples on a Bruker Avance III 400WB spectrometer at the resonance frequency of 104.3 MHz. The spectra were recorded upon  $\pi/6$  single pulse excitation, with the repetition time of 0.5 s, and the sample spinning rate of 8 kHz.

The acid strength of zeolite supports was determined by the <sup>1</sup>H MAS NMR with deuterated acetonitrile (CD<sub>3</sub>CN) as a probe molecule. The

spectra were recorded on a Bruker Avance III 400WB spectrometer at the resonance frequency of 400.1 MHz, with  $\pi/2$  single pulse excitation and the repetition time of 10 s. The samples for characterization were fully dehydrated, loaded with acetonitrile-d<sub>3</sub> (99.9% deuterated) and evacuated at 25 °C for 1 h to eliminate physisorbed acetonitrile.

### 2.3. Catalytic study

The CH<sub>4</sub>-SCR reaction was performed in a fixed-bed micro-reactor at atmospheric pressure. Typically, 0.12 mL catalyst sample (20–40 mesh) was placed in a quartz reactor and pretreated in 10% O<sub>2</sub>/Ar at 450 °C for 1 h. After cooling to designated temperature in He, the reactant gas mixture (typically 2500 ppm NO, 4000 ppm CH<sub>4</sub>, 4% O<sub>2</sub>, 6% H<sub>2</sub>O, He balance) was fed to the catalyst sample to start the reaction. The outlet gas was analyzed on-line with a NO<sub>x</sub> analyzer (Ecotech EC9841) and a gas chromatograph (Techcomp GC7900, equipped with a Plot TDX-1 packed column, a nickel conversion furnace and a FID detector for the analysis of CH<sub>4</sub> and CO<sub>x</sub>, as well as a Porapak Q packed column and a TCD detector for the analysis of N<sub>2</sub>O and N<sub>2</sub>). During the reaction, the outlet gas was also analyzed with a Pfeiffer Omnistar GSD 320 mass spectrometer, and the following mass fragments sensible to the system perturbation were monitored: CH<sub>4</sub> (m/e = 16), NO (m/e = 30), NO<sub>2</sub> (m/e = 46), O<sub>2</sub> (m/e = 32), N<sub>2</sub> (m/e = 28), N<sub>2</sub>O/CO<sub>2</sub> (m/e = 44), HCHO (m/e = 29). The NO and CH<sub>4</sub> conversions are defined as follows:

$$\text{NO conversion}(\%) = \frac{[\text{NO}]_{\text{inlet}} - [\text{NO}]_{\text{outlet}}}{[\text{NO}]_{\text{inlet}}} \times 100\%$$

$$\text{NO conv. to N}_2(\%) = \frac{2 \times [\text{N}_2]_{\text{outlet}}}{[\text{NO}]_{\text{inlet}}} \times 100\%$$

$$\text{NO conv. to NO}_2(\%) = \frac{[\text{NO}_2]_{\text{outlet}}}{[\text{NO}]_{\text{inlet}}} \times 100\%$$

$$\text{CH}_4 \text{ conversion}(\%) = \frac{[\text{CH}_4]_{\text{inlet}} - [\text{CH}_4]_{\text{outlet}}}{[\text{CH}_4]_{\text{inlet}}} \times 100\%$$

$$\text{CH}_4 \text{ conv. to CO}_2(\%) = \frac{[\text{CO}_2]_{\text{outlet}}}{[\text{CH}_4]_{\text{inlet}}} \times 100\%$$

### 2.4. Temperature-programmed desorption analysis

The temperature-programmed desorption (TPD) experiments were performed on the fixed-bed micro-reactor at atmospheric pressure. In a typical process, 0.12 mL catalyst sample was placed in a quartz reactor, pretreated in 10% O<sub>2</sub>/Ar at 450 °C for 1 h, and then cooled down to 50 °C in flowing He. The gas mixture, i.e. 1%CH<sub>4</sub>-99%He, 1%NO-99%He, 1%NO-10%O<sub>2</sub>-89%He or 1%NO<sub>2</sub>-99%He, was fed to the catalyst sample for saturated adsorption at 50 °C. After purging with He for 1 h to remove the weakly adsorbed species, the TPD profiles were recorded in flowing He (20 mL/min) at a heating rate of 10 °C/min. The desorption products were on-line analyzed with the Pfeiffer Omnistar GSD 320 mass spectrometer.

## 3. Results

### 3.1. Catalyst characterization

The XRD patterns of H-SSZ-13 and supported catalysts are shown in Fig. S1. All samples exhibited typical diffraction lines corresponding to CHA zeolite topology. Besides, no characteristic diffraction lines of Ru and/or In species could be observed, probably due to the low loadings of metal species and their good dispersion. In the SEM image of 0.5% Ru-2%In/H-SSZ-13, the homogeneous dispersion of Ru and In species on zeolite support was clearly observed in the micrometer scale (Fig. S2). EDS analysis revealed the weight loadings of 0.5 and 2.0% for Ru and In, respectively, which matched perfectly well with the target

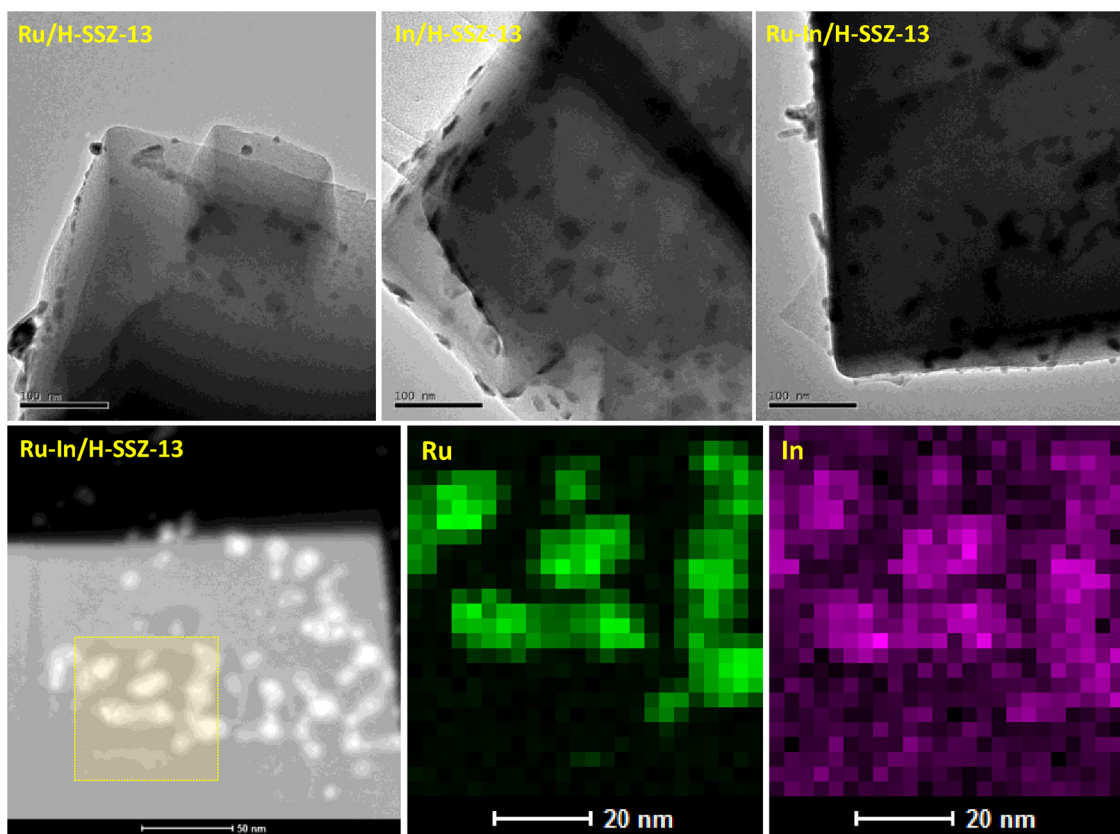


**Fig. 1.** TEM images of 0.5%Ru/H-SSZ-13, 2%In/H-SSZ-13 and 0.5%Ru-2%In/H-SSZ-13, and HAADF-STEM image of 0.5%Ru-2%In/H-SSZ-13 with corresponding element mapping.

values.

For a direct observation of Ru and In species on H-SSZ-13 zeolite in the nanometric scale, TEM analysis was performed. As shown in Fig. 1, dark spherical spots (4–20 nm) corresponding to Ru species were dispersed on zeolite support of 0.5%Ru/H-SSZ-13 and irregular polygon-like particles (6–30 nm) corresponding to In species were dispersed on zeolite support of 2%In/H-SSZ-13. While for 0.5%Ru-2%In/H-SSZ-13, worm-like dark particles with sizes of 10–20 nanometers were observed to be dispersed both on the outer surfaces and inside zeolite crystals. The HAADF-STEM element mapping images clearly revealed that Ru and In nanoparticles (~10 nm) located in the same regions in 0.5%Ru-2%In/H-SSZ-13. That is, the close contact between Ru and In species was achieved. Considering the fact that both Ru and In species should exist in most thermodynamically stable states on H-SSZ-13 support through reduction-oxidation treatments at elevated temperatures (see experiment section for details), the close contact between Ru and In species should originate from their intrinsic physicochemical properties as well as the support effects of H-SSZ-13 zeolite.

The oxidation states of Ru and In species in selected samples (after reduction-oxidation treatments) were characterized by XPS. As shown in Fig. 2, binding energy value at 281.1 eV corresponding to  $3d_{5/2}$  of  $\text{RuO}_2$  [45,46] was observed for 0.5%Ru/H-SSZ-13. For 2%In/H-SSZ-13, binding energy values at 453.9 and 446.5 eV corresponding to the  $3d_{3/2}$  and  $3d_{5/2}$  of  $(\text{InO})^+$  and/or  $\text{In}_2\text{O}_3$  species [28,47] were observed. In the case of bimetallic 0.5%Ru-2%In/H-SSZ-13 sample, the Ru  $3d_{5/2}$  binding energy value shifted by -0.2 eV when compared with that of monometallic 0.5%Ru/H-SSZ-13 while the In  $3d_{5/2}$  binding energy value shifted by +0.2 eV when compared with that of monometallic 2%In/H-SSZ-13. These small shifts in binding energy values did not point to different oxidation states of Ru and In species, but indicated the electronic interaction between Ru and In (with electron transfer), which was a logical result from their close contact as revealed by TEM analysis

(Fig. 1).

The oxidation states and redox properties of Ru and In species were further characterized by means of temperature-programmed reduction. As shown in Fig. 3, the complete reduction of different types of  $\text{RuO}_2$  to  $\text{Ru}^\circ$  ( $\text{H/Ru} = \sim 4$ ) occurred in the temperature range of 100–200 °C in 0.5%Ru/H-SSZ-13 [48]. The reduction of  $\text{In}^{3+}$  to  $\text{In}^+$  species ( $\text{H/In} = \sim 2$ ) was observed in 2%In/H-SSZ-13 with a broad hydrogen consumption peak centered at 290 °C [47,49]. While for bimetallic 0.5%Ru-2%In/H-SSZ-13, the reduction of  $\text{In}^{3+}$  species shifted slightly toward lower temperature (275 °C,  $\text{H/In} = \sim 2$ ) and the dominating reduction of  $\text{RuO}_2$  species shifted distinctly toward higher temperature (230 °C,  $\text{H/Ru} = \sim 3$ ) compared with monometallic sample. The  $\text{H}_2$ -TPR profiles confirmed the electronic interaction between Ru and In species in 0.5%Ru-2%In/H-SSZ-13, as indicated by XPS analysis. The presence of In species with close contact retarded the reduction of Ru species and the presence of Ru species promoted the reduction of In species.

With the above-mentioned characterization data, it can be concluded that bimetallic 0.5%Ru-2%In/H-SSZ-13 with close contact and electronic interaction between Ru and In species has been successfully prepared via the wet impregnation followed by reduction-oxidation treatment.

### 3.2. Screening of catalyst for $\text{CH}_4$ -SCR

H-SSZ-13 zeolite support exhibited very low activity in  $\text{CH}_4$ -SCR with neglectable NO conversion to  $\text{N}_2$  at 500 °C. Introduction of In species to H-SSZ-13 dramatically enhanced the  $\text{CH}_4$ -SCR activity, which appeared to somewhat dependent on In loadings. With increasing In loadings from 1 to 4%, the NO conversion to  $\text{N}_2$  first increased and then decreased while  $\text{CH}_4$  conversion to  $\text{CO}_2$  kept increasing. The highest NO conversion to  $\text{N}_2$  of 37% with  $\text{CH}_4$  conversion to  $\text{CO}_2$  of 32% at 500 °C

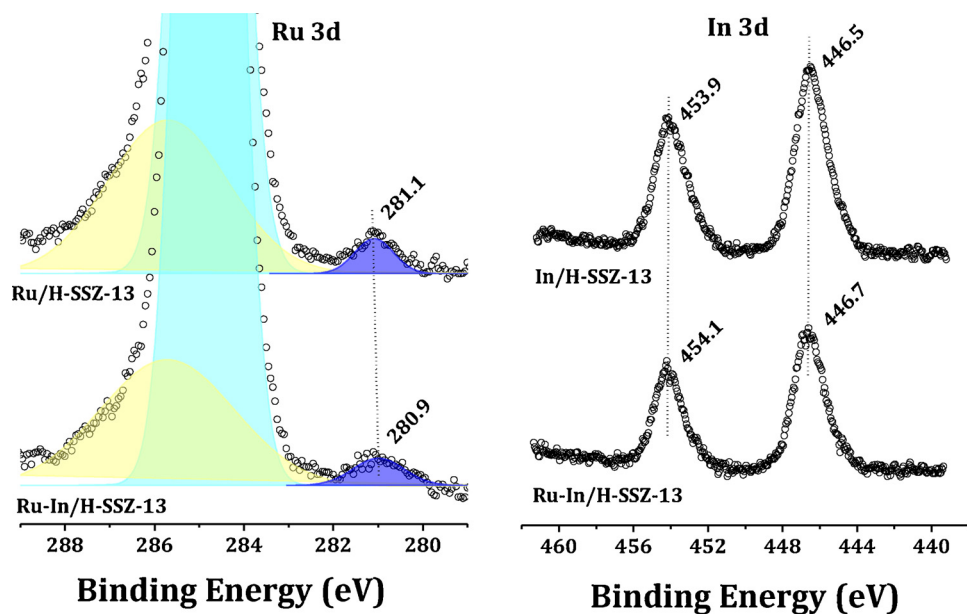


Fig. 2. Ru 3d and In 3d XPS of 0.5%Ru/H-SSZ-13, 2%In/H-SSZ-13 and 0.5%Ru-2%In/H-SSZ-13.

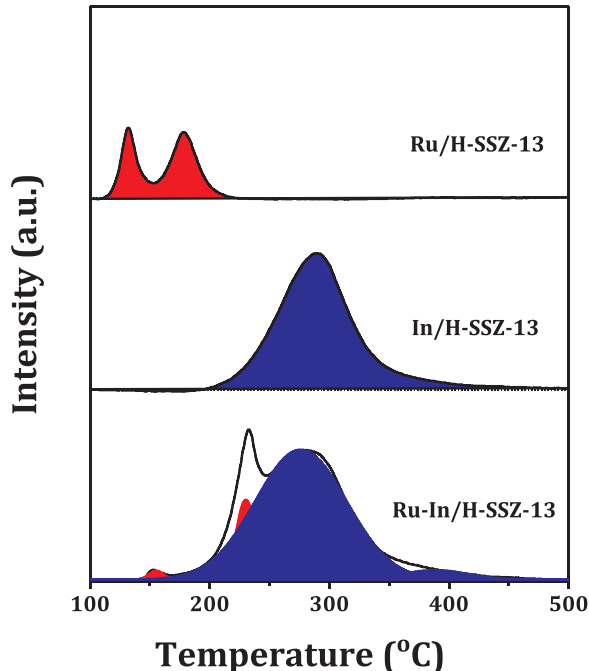


Fig. 3. H<sub>2</sub>-TPR profiles of 0.5%Ru/H-SSZ-13, 2%In/H-SSZ-13 and 0.5%Ru-2%In/H-SSZ-13.

was achieved with the optimized 2%In/H-SSZ-13 under employed harsh conditions. 2%In/H-SSZ-13 was established as a reference catalyst and a second element was further introduced to promote its CH<sub>4</sub>-SCR activity. As shown in Fig. 4, some elements, i.e. Cr, Ce and Ru, showed significant promotion effects on NO reduction to N<sub>2</sub> while others not. Even if 0.5%Ru/H-SSZ-13 exhibited very limited activity in CH<sub>4</sub>-SCR, Ru appeared to be the best modifier for 2%In/H-SSZ-13 and the promotion effect of Ru will be discussed in the following section. With optimized Ru loading of 0.5%, NO conversion to N<sub>2</sub> of 90% with CH<sub>4</sub> conversion to CO<sub>2</sub> of 66% was achieved at 500 °C, which appeared to be very attractive results for CH<sub>4</sub>-SCR under comparable reaction conditions [20–22,33,50].

With 0.5%Ru-2%In as optimized active components, the effects of

zeolite supports were examined, as shown in Figs S3 & 4. It is interesting to reveal that the topology of aluminosilicate zeolites played a key role in controlling the CH<sub>4</sub>-SCR activity of supported 0.5%Ru-2%In catalysts (prepared via similar procedures). H-SSZ-13 appeared to be the best support, followed by H-ZSM-5, then H-beta and H-mordenite. With the same topology of CHA, aluminosilicate H-SSZ-13 seemed to be a much better support for 0.5%Ru-2%In than silicoaluminophosphate SAPO-34. According to these observations, both the topology and the chemical constitution of zeolite supports could significantly influence the CH<sub>4</sub>-SCR activity of supported 0.5%Ru-2%In active components.

For a better understanding of bimetallic 0.5%Ru-2%In/H-SSZ-13 for CH<sub>4</sub>-SCR, its temperature-dependent catalytic performance, together with 0.5%Ru/H-SSZ-13 and 2%In/H-SSZ-13, are shown in Fig. 5. 0.5%Ru/H-SSZ-13 exhibited considerable activity in the low temperature range (200–300 °C), and both NO<sub>2</sub> and N<sub>2</sub> could be detected as products from NO conversion. Since neglectable amount of CH<sub>4</sub> was converted in this temperature range, the products should come from NO oxidation (2NO + O<sub>2</sub> → 2NO<sub>2</sub>) and decomposition (2NO → N<sub>2</sub> + O<sub>2</sub>), which had been reported to be the unique nature of Ru catalysts [51]. With increasing temperature from 400 to 550 °C, the NO conversion over 0.5%Ru/H-SSZ-13 gradually decreased. 2%In/H-SSZ-13 also exhibited noticeable activity in CH<sub>4</sub>-SCR and the activity increased with increasing reaction temperature from 200 to 550 °C. In the high temperature range, N<sub>2</sub> was detected as an exclusive product, which should come from NO selective reduction by CH<sub>4</sub> (2NO + CH<sub>4</sub> + O<sub>2</sub> → N<sub>2</sub> + 2H<sub>2</sub>O + CO<sub>2</sub>). Bimetallic 0.5%Ru-2%In/H-SSZ-13 acted more like 0.5%Ru/H-SSZ-13 at < 400 °C, while a synergistic effect between Ru and In species was clearly demonstrated in the high temperature range, i.e. NO conversion to N<sub>2</sub> was much higher than the sum of those achieved with 0.5%Ru/H-SSZ-13 and 2%In/H-SSZ-13.

The reactions of NO oxidation and CH<sub>4</sub> oxidation over 0.5%Ru/H-SSZ-13, 2%In/H-SSZ-13 and 0.5%Ru-2%In/H-SSZ-13 were investigated. As shown in Fig. 6 (left-hand chart), 2%In/H-SSZ-13 exhibited very low activity for NO oxidation (NO conversion below 10% at 200–450 °C) while 0.5%Ru/H-SSZ-13 appeared to be very active for NO oxidation, consistent with our previous work on Ru catalysts [48,52]. 0.5%Ru-2%In/H-SSZ-13 acted like 0.5%Ru/H-SSZ-13 in NO oxidation, but it exhibited lower activity in the temperature range of 200–300 °C. For CH<sub>4</sub> oxidation, all the three catalysts showed increasing activity with increasing reaction temperature from 350 to

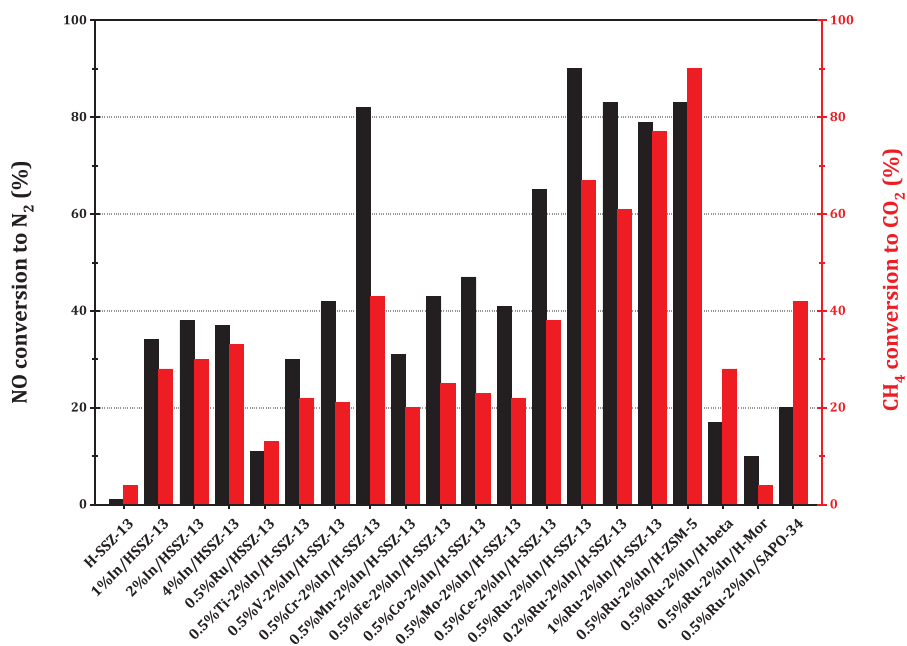


Fig. 4. Screening of catalyst for CH<sub>4</sub>-SCR. Reaction conditions: 2500 ppm NO, 4000 ppm CH<sub>4</sub>, 4% O<sub>2</sub>, 6% H<sub>2</sub>O, He balance; T = 500 °C; GHSV = 75,000 h<sup>-1</sup>.

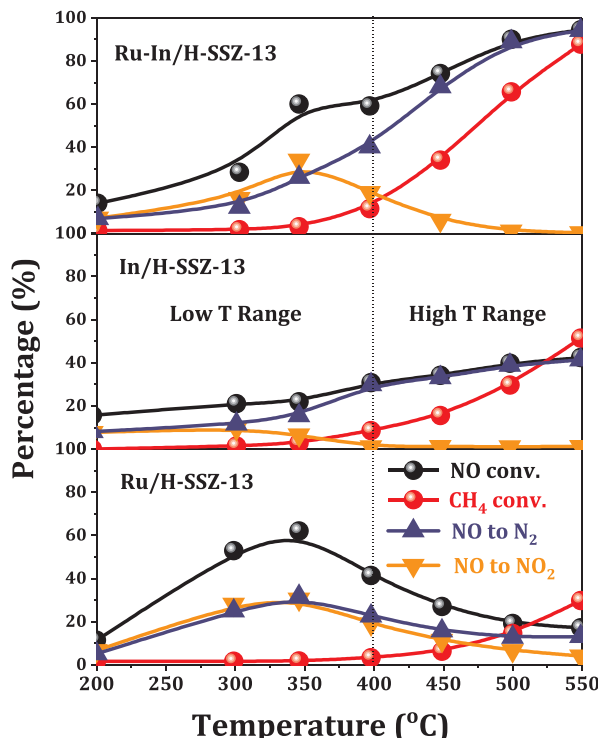


Fig. 5. CH<sub>4</sub>-SCR over 0.5%Ru/H-SSZ-13, 2%In/H-SSZ-13 and 0.5%Ru-2%In/H-SSZ-13. Reaction conditions: 2500 ppm NO, 4000 ppm CH<sub>4</sub>, 4% O<sub>2</sub>, 6% H<sub>2</sub>O, He balance; GHSV = 75,000 h<sup>-1</sup>.

550 °C. And In-containing samples, i.e. In/H-SSZ-13 and Ru-In/H-SSZ-13, appeared to be more active than Ru/H-SSZ-13. It was simply speculated that NO was preferentially activated on Ru site while CH<sub>4</sub> activated on In sites. The details will be discussed with results from temperature-programmed desorption studies in the following section.

Some important reaction parameters, e.g. CH<sub>4</sub> and O<sub>2</sub> concentrations in the feeding gas and space velocity employed, were investigated, as shown in Fig. S4. Being employed as a reductant for NO, the concentration of CH<sub>4</sub> showed significant influence on NO conversion.

Typically, the NO conversion to N<sub>2</sub> (fixed NO concentration of 2500 ppm) increased with increasing CH<sub>4</sub> concentration from 800 to 4000 ppm CH<sub>4</sub>, and then leveled off with CH<sub>4</sub> concentration further increase to 5000 ppm. In this study, excess CH<sub>4</sub> of 4000 ppm was employed to promote the reduction of NO due to its cheapness and availability in gas-fired power plant. The unreacted CH<sub>4</sub> could be easily removed by catalytic combustion. In the absence of O<sub>2</sub>, considerable NO conversion to N<sub>2</sub> (~10% at 300–450 °C) could be achieved on 0.5% Ru-2%In/H-SSZ-13. When 2% O<sub>2</sub> was added to the feed gas, both the conversion of NO and CH<sub>4</sub> was significantly promoted, i.e. triggering CH<sub>4</sub>-SCR reaction. More O<sub>2</sub> of 4% could promote NO oxidation at low temperatures, but it showed little effect on CH<sub>4</sub>-SCR at high temperatures, similar to that reported by Armor [11] and Flytzani-Stephanopoulos [53]. The effect of space velocity on CH<sub>4</sub>-SCR over 0.5%Ru-2%In/H-SSZ-13 was also investigated and presented in Fig. S4. Increasing GHSV from 40,000 to 75,000 h<sup>-1</sup> showed limited effect on NO reduction, while a significant decline in NO conversion to N<sub>2</sub> at > 400 °C was observed with GHSV further increase to 120,000 h<sup>-1</sup>.

The catalyst stability is a very important issue for potential application. Since CH<sub>4</sub>-SCR is operated at high temperature (usually > 500 °C) and in excess steam, eligible stability remains challenging for CH<sub>4</sub>-SCR catalyst. The H-SSZ-13 zeolite was very stable during CH<sub>4</sub>-SCR, and no structure destruction occurred after reaction at 500 °C for 48 h, as revealed by the characterization results from XRD, <sup>27</sup>Al MAS NMR and Ar adsorption-desorption isotherms (Figs. S1, S5 & S6). In this work, it is amazing to disclose for the first time that the NO conversion to N<sub>2</sub> catalyzed by 0.5%Ru-2%In/H-SSZ-13 gradually increased with reaction time at 500 °C, i.e. from 85 to 95% within 12 h (Fig. 7). These observations should be explained from the re-construction of active sites under CH<sub>4</sub>-SCR conditions. Although the 0.5%Ru-2%In active components should exist in the most thermodynamically stable states on H-SSZ-13 support after reduction-oxidation treatments at elevated temperatures, the re-construction might occur with the presence of CH<sub>4</sub> and NO in the feeding gas. Fortunately, this type of site re-construction was beneficial to CH<sub>4</sub>-SCR reaction. The presence of 6% H<sub>2</sub>O showed neglectable effect on CH<sub>4</sub>-SCR, which is also amazing for CH<sub>4</sub>-SCR catalyst.

According to the catalytic data, it can be stated that bimetallic 0.5% Ru-2%In/H-SSZ-13 behaves as eligible CH<sub>4</sub>-SCR catalyst with high activity and good stability under harsh reaction conditions.

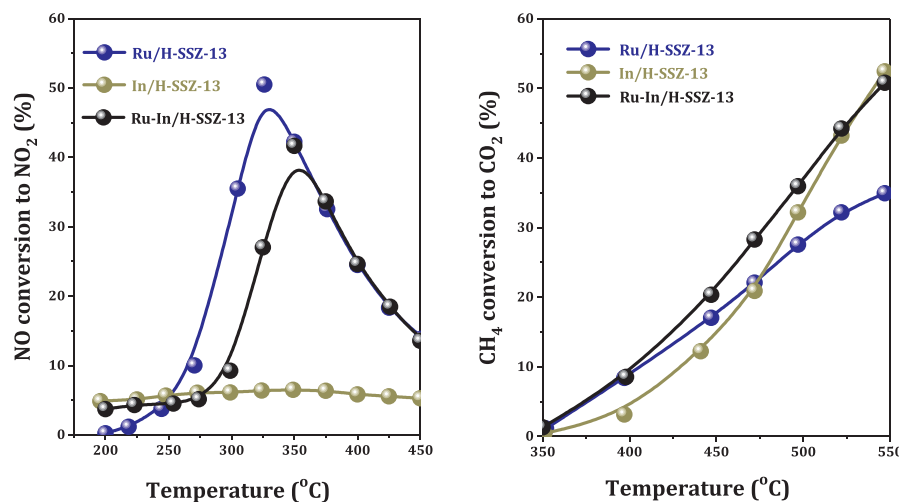


**Fig. 6.** NO and CH<sub>4</sub> oxidation over 0.5%Ru/H-SSZ-13, 2%In/H-SSZ-13 and 0.5%Ru-2%In/H-SSZ-13. Reaction conditions: 2500 ppm NO or 4000 ppm CH<sub>4</sub>, 4% O<sub>2</sub>, 6% H<sub>2</sub>O, He balance; GHSV = 75,000 h<sup>-1</sup>.

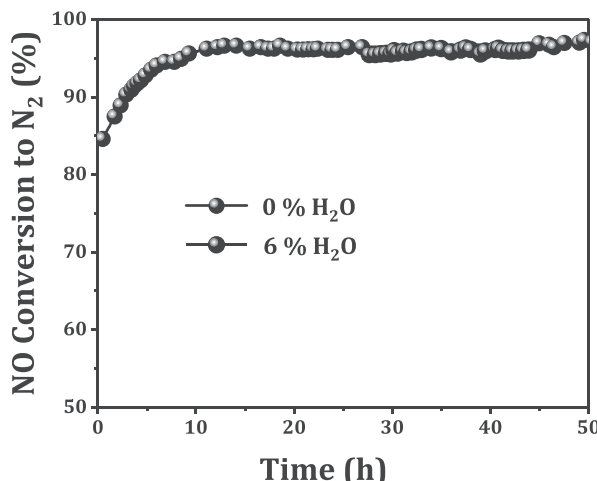


**Fig. 7.** Stability test of 0.5%Ru-2%In/H-SSZ-13 in CH<sub>4</sub>-SCR. Reaction conditions: 2500 ppm NO, 4000 ppm CH<sub>4</sub>, 4% O<sub>2</sub>, 0 or 6% H<sub>2</sub>O, He balance; T = 500 °C, GHSV = 75,000 h<sup>-1</sup>.

### 3.3. Temperature-programmed desorption studies

For an insight into CH<sub>4</sub>-SCR catalyzed by 0.5%Ru-2%In/H-SSZ-13, the possible surface species and their stability under various conditions were investigated by means of temperature-programmed desorption technique.

The desorption of CH<sub>4</sub> was firstly investigated. As shown in Fig. S7, CH<sub>4</sub> desorption started from 125 °C, centered at 220 °C and ended at ~400 °C on H-SSZ-13. During the desorption process, no intermediates from CH<sub>4</sub> activation, e.g. CH<sub>3</sub>OH, HCHO and CO<sub>x</sub>, could be detected. Since no significant CH<sub>4</sub> desorption peak was observed on Na-SSZ-13 (Fig. S7), the strong interaction between CH<sub>4</sub> and the bridging hydroxyls Si—OH-Al, i.e. Brønsted acid sites in zeolite, could be proposed. As shown in Fig. 8, the CH<sub>4</sub>-TPD profiles on 0.5%Ru/H-SSZ-13, 2%In/H-SSZ-13 and 0.5%Ru-2%In/H-SSZ-13 were somewhat similar to that observed on H-SSZ-13 (in terms of adsorbing capacity and desorption temperature), implying that CH<sub>4</sub> adsorption occurred dominantly on the Brønsted acid sites in zeolite. While different to that observed on H-SSZ-13, a small but detectable amount of intermediates from CH<sub>4</sub> activation, namely HCHO and CO<sub>2</sub>, could be observed. A rational explanation was that CH<sub>4</sub>, which was adsorbed on the Brønsted acid sites, could be oxidized by the adsorbed oxygen and/or lattice oxygen on

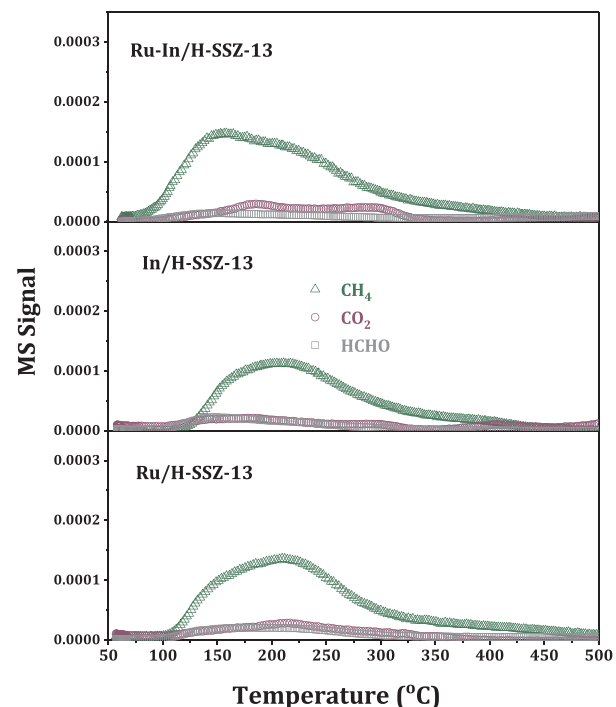


**Fig. 8.** Temperature-programmed desorption of CH<sub>4</sub> on 0.5%Ru/H-SSZ-13, 2%In/H-SSZ-13 and 0.5%Ru-2%In/H-SSZ-13 catalysts.

adjacent Ru, In or Ru-In sites.

NO, NO-O<sub>2</sub> and NO<sub>2</sub> could adsorb on H-SSZ-13 in the form of N<sub>x</sub>O<sub>y</sub> species via interaction with acidic hydroxyls in zeolite. All these adsorbed N<sub>x</sub>O<sub>y</sub> species underwent escape from H-SSZ-13 below 200 °C (Fig. S8), with NO and NO<sub>2</sub> detected as desorption and/or decomposition products [54]. Obviously, these unstable N<sub>x</sub>O<sub>y</sub> species could not be utilized in CH<sub>4</sub>-SCR in the high temperature range (400–550 °C), corresponding to the very low CH<sub>4</sub>-SCR activity of H-SSZ-13. The NO-TPD profiles on 0.5%Ru/H-SSZ-13, 2%In/H-SSZ-13 and 0.5%Ru-2%In/H-SSZ-13 are shown in Fig. 9 left-hand chart. Only a weak NO desorption peak centered at 140 °C was observed on 0.5%Ru/H-SSZ-13, corresponding to the desorption of unstable N<sub>x</sub>O<sub>y</sub> species. For 2%In/H-SSZ-13, both a weak NO desorption peak at 50–150 °C and a strong NO desorption peak at 250–450 °C were observed. Moreover, NO<sub>2</sub>, N<sub>2</sub>O and O<sub>2</sub> were detected together with NO desorption at high temperature.

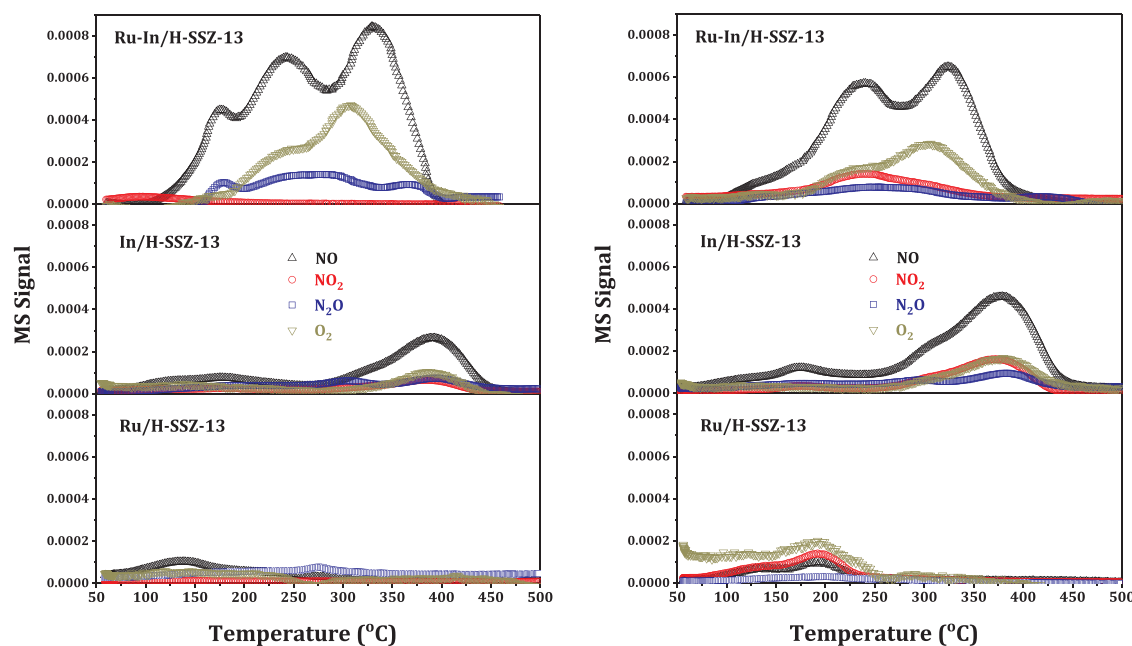
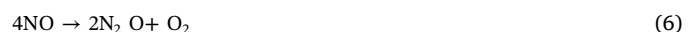


**Fig. 9.** Temperature-programmed desorption of NO (left) and NO-O<sub>2</sub> (right) on 0.5%Ru/H-SSZ-13, 2%In/H-SSZ-13 and 0.5%Ru-2%In/H-SSZ-13 catalysts.

According to these observations, it was proposed that NO could be oxidized by adsorbed oxygen and lattice oxygen from In species to nitrite (Eq. (1)) or nitrate (Eq. (2)) species, which underwent decomposition to release NO, NO<sub>2</sub>, N<sub>2</sub>O and O<sub>2</sub> at high temperatures Eqs. (3)–(6). Please note that the thermodynamic control will also affect the observed ratio of NO/NO<sub>2</sub> at > 300 °C. The stable N<sub>x</sub>O<sub>y</sub> species on In sites could reaction with CH<sub>4</sub> on adjacent Brønsted acid sites, which was responsible for the CH<sub>4</sub>-SCR activity of 2%In/H-SSZ-13. While for bimetallic 0.5%Ru-2%In/H-SSZ-13, multiple NO desorption peaks were observed in the temperature range of 120–400 °C. N<sub>2</sub>O and O<sub>2</sub> signals were detected together with NO signal while almost no NO<sub>2</sub> signal could be detected. Obviously, Ru species promoted the oxidative activation of NO (Eq. (7)) and the formation of nitrite or nitrate species on adjacent In sites (Eqs. (8) & (9)). On the other hand, Ru could also promote the decomposition of NO<sub>2</sub> and, therefore, no NO<sub>2</sub> was detected as desorption product on 0.5%Ru/H-SSZ-13 and 0.5%Ru-2%In/H-SSZ-13 (Fig. 9 left-hand chart). It means that the NO<sub>2</sub> from NO oxidation on Ru sites must be stored in adjacent In sites in the form of N<sub>x</sub>O<sub>y</sub> species, otherwise it would undergo reversible decomposition to NO, i.e. the case of 0.5%Ru/H-SSZ-13. To confirm these hypotheses, NO<sub>2</sub>-TPD experiments were performed and the results were shown in Fig. S9. From NO<sub>2</sub>-TPD profile on 0.5%Ru/H-SSZ-13, the role of Ru in promoting NO<sub>2</sub> decomposition at low temperatures (Eq. (5)) could be clearly demonstrated. Comparing NO<sub>2</sub>-TPD and NO-TPD profiles on 2%In/H-SSZ-13, it could be concluded that the adsorption and storage of NO<sub>2</sub> were more easily than NO on In sites. While the introduction of Ru species could promote the adsorption and storage of both NO and NO<sub>2</sub> (Fig. 9 left-hand chart & Fig. S9). That is, NO and NO<sub>2</sub> should first interact with Ru sites and then migrate to adjacent In sites in the form of N<sub>x</sub>O<sub>y</sub>.

The TPD profiles of NO-O<sub>2</sub> on 0.5%Ru/H-SSZ-13, 2%In/H-SSZ-13 and 0.5%Ru-2%In/H-SSZ-13 were final investigated, as shown in Fig. 9 right-hand chart. O<sub>2</sub> signal, with intensity higher than NO and NO<sub>2</sub>, was detected at low temperature of 50–250 °C on 0.5%Ru/H-SSZ-13, corresponding to the desorption of chemisorbed oxygen on Ru sites. Meanwhile, more NO<sub>2</sub> was detected than NO in the TPD profile of NO-O<sub>2</sub>, indicating the good NO oxidation activity of Ru as revealed by NO oxidation experiment (Fig. 6). Even though 0.5%Ru/HSSZ-13 was very active in NO oxidative activation, the formed NO<sub>2</sub> could not be stored in the form of stable N<sub>x</sub>O<sub>y</sub> species, which was key reason for the low activity of 0.5%Ru/HSSZ-13 in CH<sub>4</sub>-SCR in the high temperature range.

For 2%In/H-SSZ-13, stable N<sub>x</sub>O<sub>y</sub> species were stored on In sites, which underwent decomposition to NO, NO<sub>2</sub>, N<sub>2</sub>O and O<sub>2</sub> at 250–450 °C (Eqs. (3)–(6)). Comparing the TPD profiles of NO and NO-O<sub>2</sub> (Fig. 9), the presence of O<sub>2</sub> promoted the oxidative activation of NO and the subsequent storage of N<sub>x</sub>O<sub>y</sub> species on In sites. In could catalyzed the oxidation of NO, but much less active than Ru (Fig. 6). In this context, the introduction of Ru sites with high activity for NO oxidative activation could promote the storage of stable N<sub>x</sub>O<sub>y</sub> species on In sites, in case of free migration of N<sub>x</sub>O<sub>y</sub> species from Ru to In sites. It is very interesting to disclose that the Ru-In system reported here acts very much like a lean NO<sub>x</sub> trap, e.g. Pt/BaO/Al<sub>2</sub>O<sub>3</sub> [44,55,56].



#### 4. Discussion

According to the catalytic data, bimetallic 0.5%Ru-2%In/H-SSZ-13 has been successfully developed as a robust catalyst for CH<sub>4</sub>-SCR. However, it is more important to know the origin of the remarkable CH<sub>4</sub>-SCR activity of 0.5%Ru-2%In/H-SSZ-13, which should shed a light on future catalyst design. In the following section, we will focus on the individual role of H-SSZ-13 support, In sites and Ru sites as well as their cooperation during CH<sub>4</sub>-SCR reaction.

##### 4.1. Role of H-SSZ-13 in CH<sub>4</sub>-SCR

As stated in the introduction section, zeolites are widely employed

as support materials for SCR catalysts [4,6,12,35–37]. Zeolites in their proton forms can provide strong Brønsted acid sites that can be utilized for SCR, especially for NH<sub>3</sub>-SCR [57,58]. On the other hand, zeolites can be viewed as ideal scaffolds for redox centers for SCR reactions. The properties of redox centers can be modulated by zeolite micro-environment, offering the possibility of activity modulation. Recently, the small-pore zeolites, e.g. H-SSZ-13, attract special attention in NH<sub>3</sub>-SCR due to their good stability against framework dealumination. In this work, H-SSZ-13 zeolite was selected as the support to meet the stability requirement for CH<sub>4</sub>-SCR operating at high temperature and in excess steam. Indeed, good stability was achieved with 0.5%Ru-2%In/H-SSZ-13, as shown in Fig. 7. Meanwhile, the Brønsted acid centers in zeolite supports could provide necessary sites for CH<sub>4</sub> adsorption, as revealed by CH<sub>4</sub>-TPD profiles in Figs. S7 & 8. On the other hand, zeolite supports seemed to show decisive impacts on the CH<sub>4</sub>-SCR activity, as indicated in Figs. S3 & 4. With similar Si/Al ratios, H-SSZ-13 appeared to be the best support for Ru-In active components, followed by H-ZSM-5, then H-beta and H-mordenite. H-SSZ-13, H-beta and H-mordenite showed similar Brønsted acidity, as confirmed by the very similar low-field-shifted of <sup>1</sup>H MAS NMR signal of Si(OH)Al groups after CD<sub>3</sub>CN adsorption ( $\Delta\delta_{1H} = 6.5$  ppm, Fig. S10) [59,60]. In this context, the zeolite topology was responsible for the difference in CH<sub>4</sub>-SCR activity. The small-pore H-SSZ-13 behaved as better scaffold for Ru-In than medium-pore H-beta and large-pore H-mordenite, and the close contact and electron interaction between Ru and In species were guaranteed on H-SSZ-13 (Fig. 1–3). With the same CHA topology, silicoaluminophosphate SAPO-34 was not as good support as H-SSZ-13 (Fig. S3). As indicated by <sup>1</sup>H MAS NMR of CD<sub>3</sub>CN adsorption, the Brønsted acidity of SAPO-34 ( $\Delta\delta_{1H} = 5.6$  ppm) was distinctly lower than that of H-SSZ-13 ( $\Delta\delta_{1H} = 6.5$  ppm), which should be related with their activity difference (H-SSZ-13 appeared to be more hydrophilic than SAPO-34, as revealed by water uptake experiments in Fig. S11). That was, stronger Brønsted acidity was good for CH<sub>4</sub> adsorption and activation, therefore, leading to higher CH<sub>4</sub>-SCR activity. According to our experiment observations, both the topology and the acidity of zeolite supports could show significant impacts on the activity of CH<sub>4</sub>-SCR catalysts by modulation of CH<sub>4</sub> adsorption and the existing states of supported redox centers. Besides, good hydrothermal stability of zeolite was required to prevent the catalyst deactivation caused by dealumination.

#### 4.2. Role of in sites in CH<sub>4</sub>-SCR

In-containing zeolites have been reported to be active CH<sub>4</sub>-SCR catalysts [23–29], while the origin of their unique catalytic performance is not fully understood yet. For 2%In/H-SSZ-13 and 0.5%Ru-2%In/H-SSZ-13, the adsorption of CH<sub>4</sub> was disclosed to occur on the Brønsted acid sites of zeolites (Fig. 8). In this context, the major role of In sites in CH<sub>4</sub>-SCR was more likely to be associated with NO. The TPD profiles of NO, NO<sub>2</sub> and NO-O<sub>2</sub> revealed the formation of stable N<sub>x</sub>O<sub>y</sub> species on In sites (Figs. 9 & S9), which could participate in the reaction with adsorbed CH<sub>4</sub> or secondary products from CH<sub>4</sub> activation to trigger CH<sub>4</sub>-SCR. In the absence of O<sub>2</sub>, NO could be oxidized by the lattice oxygen from In sites and stored on 2%In/H-SSZ-13 in the form of stable nitrite and nitrate species (Fig. 9, Eqs. (1) & (2)). 2%In/H-SSZ-13 also exhibited considerable activity for NO oxidation to NO<sub>2</sub> in a wide temperature range (~20% conversion at 200–450 °C, Fig. 6), and the oxidation of NO to NO<sub>2</sub> could significantly promote its storage (see comparison between NO-TPD and NO<sub>2</sub>-TPD profiles in Figs. 9 & F S9). According to the above-mentioned results, the major role of In sites in CH<sub>4</sub>-SCR was to store N<sub>x</sub>O<sub>y</sub>, e.g. nitrite and nitrate species, for CH<sub>4</sub>-SCR. The formation of high-temperature stable N<sub>x</sub>O<sub>y</sub> species (most probably bridging and bidentate nitrates [61]) was essential for the CH<sub>4</sub>-SCR activity in the high-temperature range. To realize the reaction between N<sub>x</sub>O<sub>y</sub> on In sites and CH<sub>4</sub> on the Brønsted acid sites of zeolite, suitable spatial distance between In sites and Brønsted acid sites was required, which should be a problem related with zeolite topology and

preparation route. In our study, no evidence on the direct participation of In sites in CH<sub>4</sub> activation was obtained.

#### 4.3. Role of Ru sites in CH<sub>4</sub>-SCR

Though NO<sub>2</sub> could be more easily stored on In sites than NO (Figs. 9 & S9), In sites themselves showed relatively low activity toward NO oxidation (Fig. 6). Therefore, promoting the oxidation of NO to NO<sub>2</sub> should be a feasible strategy to enhancing NO storage on In sites and facilitating the subsequent reaction between N<sub>x</sub>O<sub>y</sub> with CH<sub>4</sub>. In fact, modifications of In-containing zeolites by a second transition metal with aim to promote the oxidative activation of NO during CH<sub>4</sub>-SCR have been well documented [30–34]. In this work, Ru was selected as a promoter for In/H-SSZ-13 due to the excellent activity of Ru catalysts in NO oxidation [48]. As shown in Fig. 6, the introduction of Ru to In/H-SSZ-13 significantly promoted NO oxidation to NO<sub>2</sub> as expected. However, the further reaction between NO<sub>2</sub> and CH<sub>4</sub> was slow and considerable amount of NO<sub>2</sub> was therefore detected as byproduct from CH<sub>4</sub>-SCR in the low temperature range (Fig. 5). The results from NO<sub>2</sub>-CH<sub>4</sub> reaction over 0.5%Ru-2%In/H-SSZ-13 definitely confirm this hypothesis (Fig. S12). The TPD profiles of NO, NO<sub>2</sub> and NO-O<sub>2</sub> on 0.5%Ru/H-SSZ-13 revealed that NO<sub>2</sub> from NO oxidation could not be stored on Ru sites and underwent reversible decomposition at < 250 °C (Figs. 9 & S9). This can well explain the low CH<sub>4</sub>-SCR activity of 0.5%Ru/H-SSZ-13 in the high temperature range (Fig. 5). While in the case of 0.5%Ru-2%In/H-SSZ-13, the NO<sub>2</sub> from NO oxidation on Ru sites could migrate to adjacent In sites and be stored in the form of stable N<sub>x</sub>O<sub>y</sub> species, which could be utilized for the reaction with CH<sub>4</sub> during CH<sub>4</sub>-SCR at high temperatures. That is, the role of Ru sites in 0.5%Ru-2%In/H-SSZ-13 was to promote NO oxidation to NO<sub>2</sub>, which was further transformed to stable N<sub>x</sub>O<sub>y</sub> species on In sites. In this context, the close contact between Ru and In sites was required, which was again a problem related with zeolite topology and the preparation route.

#### 5. Conclusions

Bimetallic 0.5%In-2%In/H-SSZ-13 has been successfully constructed and applied as a robust catalyst in CH<sub>4</sub>-SCR under harsh conditions. Typically, NO conversion of ~94% with perfect N<sub>2</sub> selectivity of 100% can be achieved at 550 °C under high GHSV of 75,000 h<sup>-1</sup> and in the presence of 6% H<sub>2</sub>O, significantly outperforming monometallic 0.5%Ru/H-SSZ-13 and 2%In/H-SSZ-13. Moreover, good stability is achieved on 0.5%Ru-2%In/H-SSZ-13 and no activity loss can be observed within 50 h at 500 °C. TEM images indicate the close contact of Ru and In species in the 0.5%Ru-2%In/H-SSZ-13, and XPS and H<sub>2</sub>-TPR results confirm the electronic interaction between Ru and In species. These observations should be related to the intrinsic properties of Ru and In species as well as the support effects of H-SSZ-13.

The surface species formed and their stability on various catalysts are investigated by means of TPD and the individual roles of Ru, In and H-SSZ-13 as well as their cooperation in 0.5%Ru-2%In/H-SSZ-13 are demonstrated. H-SSZ-13 zeolite provides Brønsted acid sites for CH<sub>4</sub> adsorption at high temperatures and also acts as scaffold for Ru-In species. Ru can promote NO oxidation to NO<sub>2</sub>, which is transformed to stable N<sub>x</sub>O<sub>y</sub> species on adjacent In sites for reacting with CH<sub>4</sub> at high temperatures. This process is very similar to that observed on lean NO<sub>x</sub> traps. The cooperation between Ru, In and H-SSZ-13 zeolite is crucial for the remarkable catalytic performance of 0.5%Ru-2%In/H-SSZ-13 in CH<sub>4</sub>-SCR.

#### Acknowledgements

This work is supported by the National Natural Science Foundation of China (21773127, 21722303, 21421001) and 111 Project (B12015, B18030).

## Appendix A. Supplementary data

Supplementary material related to this article can be found, in the online version, at doi: <https://doi.org/10.1016/j.apcatb.2018.05.048>.

## References

- [1] NEC Directive Status Report 2014, EEA Technical Report, European Environment Agency, Luxembourg, 2014.
- [2] European Environment Agency, Nitrogen Oxides (NOx) Emissions, (2010), pp. 1–20.
- [3] J.J. Spivey, S.-W. Ham, I.-S. Nam, Selective catalytic reduction of nitrogen oxides by ammonia, *Catalysis* 16 (2002).
- [4] S. Brandenberger, O. Kröcher, A. Tissler, R. Althoff, The state of the art in selective catalytic reduction of NOx by ammonia using metal-exchanged zeolite catalysts, *Catal. Rev.* 50 (2008) 492–531.
- [5] J.H. Kwak, R.G. Tonkyn, D.H. Kim, J. Szanyi, C.H.F. Peden, Excellent activity and selectivity of Cu-SSZ-13 in the selective catalytic reduction of NOx with NH<sub>3</sub>, *J. Catal.* 275 (2010) 187–190.
- [6] J. Li, H. Chang, L. Ma, J. Hao, R.T. Yang, Low-temperature selective catalytic reduction of NOx with NH<sub>3</sub> over metal oxide and zeolite catalysts- a review, *Catal. Today* 175 (2011) 147–156.
- [7] C. Paolucci, J.D. Iorio, F. Ribeiro, R. Gounder, W. Schneider, Catalysis science of NOx selective catalytic reduction with ammonia over Cu-SSZ-13 and Cu-SAPO-34, *Adv. Catal.* 59 (2016) 1–107.
- [8] J. Shibata, M. Hashimoto, K. Shimizu, H. Yoshida, T. Hattori, A. Satsuma, Factors controlling activity and selectivity for SCR of NO by hydrogen over supported platinum catalysts, *J. Phys. Chem. B* 108 (2004) 18327–18335.
- [9] L. Li, P. Wu, Q. Yu, G. Wu, N. Guan, Low temperature H<sub>2</sub>-SCR over platinum catalysts supported on Ti-containing MCM-41, *Appl. Catal. B* 94 (2010) 254–262.
- [10] P.G. Savva, C.N. Costa, Hydrogen lean-DeNOx as an alternative to the ammonia and hydrocarbon selective catalytic reduction (SCR), *Catal. Rev.* 53 (2011) 91–151.
- [11] J.N. Armor, Catalytic reduction of nitrogen oxides with methane in the presence of excess oxygen: a review, *Catal. Today* 26 (1995) 147–158.
- [12] Y. Traa, B. Burger, J. Weitkamp, Zeolite-based materials for the selective catalytic reduction of NOx with hydrocarbons, *Micropor. Mesopor. Mater.* 30 (1999) 3–41.
- [13] N.W. Cant, I.O.Y. Liu, The mechanism of the selective reduction of nitrogen oxides by hydrocarbons on zeolite catalysts, *Catal. Today* 63 (2000) 133–146.
- [14] L. Li, J. Chen, S. Zhang, N. Guan, M. Richter, R. Eckelt, R. Fricke, Study on metal-MFI/cordierite as promising catalysts for selective catalytic reduction of nitric oxide by propane in excess oxygen, *J. Catal.* 228 (2004) 12–22.
- [15] L. Li, N. Guan, HC-SCR reaction pathways on ion exchanged ZSM-5 catalysts, *Micropor. Mesopor. Mater.* 117 (2009) 450–457.
- [16] R. Mrad, A. Aissat, R. Cousin, D. Courcot, S. Siffert, Catalysts for NOx selective catalytic reduction by hydrocarbons (HC-SCR), *Appl. Catal. A* 504 (2015) 542–548.
- [17] S. Tamm, H.H. Ingelsten, M. Skoglundh, A.E.C. Palmqvist, Mechanistic aspects of the selective catalytic reduction of NOx by dimethyl ether and methanol over γ-Al<sub>2</sub>O<sub>3</sub>, *J. Catal.* 276 (2010) 402–411.
- [18] F. Gunnarsson, J.A. Pihl, T.J. Toops, M. Skoglundh, H. Härelind, Lean NOx reduction over Ag/alumina catalysts via ethanol-SCR using ethanol/gasoline blends, *Appl. Catal. B* 202 (2016) 42–50.
- [19] F. Lónyi, J. Valyon, L. Gutierrez, M.A. Ulla, E.A. Lombardo, The SCR of NO with CH<sub>4</sub> over Co-, Co, Pt-, and H-mordenite catalysts, *Appl. Catal. B* 73 (2007) 1–10.
- [20] M. Takahashi, T. Nakatani, S. Iwamoto, T. Watanabe, M. Inoue, Performance of solvothermally prepared Ga<sub>2</sub>O<sub>3</sub>-Al<sub>2</sub>O<sub>3</sub> catalysts for SCR of NO with methane, *Appl. Catal. B* 70 (2007) 73–79.
- [21] F. Lónyi, H.E. Solt, Z. Pászti, J. Valyon, Mechanism of NO-SCR by methane over Co,H-ZSM-5 and Co,H-mordenite catalysts, *Appl. Catal. B* 150–151 (2014) 218–229.
- [22] A.N. Mendes, V.L. Zhlobenko, F. Thibault-Starzyk, P.D. Costa, C. Henriques, On the enhancing effect of Ce in Pd-MOR catalysts for NOx CH<sub>4</sub>-SCR: a structure-reactivity study, *Appl. Catal. B* 195 (2016) 121–131.
- [23] E. Kikuchi, M. Ogura, I. Terasaki, Y. Goto, Selective reduction of nitric oxide with methane on gallium and indium containing H-ZSM-5 catalysts: formation of active sites by solid-state ion exchange, *J. Catal.* 161 (1996) 465–470.
- [24] X.J. Zhou, Z.S. Xu, T. Zhang, L.W. Lin, The chemical status of indium in indium impregnated HZSM-5 catalysts for the SCR of NO with CH<sub>4</sub>, *J. Mol. Catal. A* 122 (1997) 125–129.
- [25] M. Ogura, T. Ohsaki, E. Kikuchi, The effect of zeolite structures on the creation of InO<sup>+</sup> active sites for NO reduction with methane, *Micropor. Mesopor. Mater.* 21 (1998) 533–540.
- [26] T. Sowade, C. Schmidt, F.W. Schütze, H. Berndt, W. Grünert, Relations between structure and catalytic activity of Ce-In-ZSM-5 catalysts for the selective reduction of NO by methane : I. The In-ZSM-5 system, *J. Catal.* 214 (2003) 100–112.
- [27] T. Maunula, J. Ahola, H. Hamada, Reaction mechanism and kinetics of NOx reduction by methane on In/ZSM-5 under lean conditions, *Appl. Catal. B* 64 (2006) 13–24.
- [28] A. Kubacka, J. Janas, B. Sulikowski, In/Co-ferrierite: a highly active catalyst for the CH<sub>4</sub>-SCR NO process under presence of steam, *Appl. Catal. B* 69 (2006) 43–48.
- [29] O.A. Anzuñiza, A.R. Beltramone, F.G. Requejo, In-containing BEA zeolite for selective catalytic reduction of NOx part I: synthesis, characterization and catalytic activity, *J. Mol. Catal. A* 267 (2007) 194–201.
- [30] T. Sowade, T. Liese, C. Schmidt, F.W. Schütze, X. Yu, H. Berndt, W. Grünert, Relations between structure and catalytic activity of Ce-In-ZSM-5 catalysts for the selective reduction of NO by methane II: Interplay between the CeO<sub>2</sub> promoter and different indium sites, *J. Catal.* 225 (2004) 105–115.
- [31] R. Serra, M.J. Vecchietti, E. Miro, A. Boix, In,Fe-zeolites: active and stable catalysts for the SCR of NOx-kinetics, characterization and deactivation studies, *Catal. Today* 133–135 (2008) 480–486.
- [32] F. Lónyi, H.E. Solt, J. Valyon, H. Decolatti, L.B. Gutierrez, E. Miró, An operando DRIFTS study of the active sites and the active intermediates of the NO-SCR reaction by methane over In,H- and In,Pd,H-zeolite catalysts, *Appl. Catal. B* 100 (2010) 133–142.
- [33] F. Lónyi, H.E. Solt, J. Valyon, A. Boix, L.B. Gutierrez, The SCR of NO with methane over In,H- and Co,In,H-ZSM-5 catalysts: the promotional effect of cobalt, *Appl. Catal. B* 117–118 (2012) 212–223.
- [34] H.P. Decolatti, E.G. Giuria, S.N. Ibarlín, N. Navascues, S. Irusta, E.E. Miro, L.B. Gutierrez, Exchanged lanthanum in InHMOR and its impact on the catalytic performance of InHMOR spectroscopic, volumetric and microscopic studies, *Micropor. Mesopor. Mater.* 222 (2016) 9–22.
- [35] M. Li, Y. Yeom, E. Weitz, W.M.H. Sachtle, Possible reasons for the superior performance of zeolite-based catalysts in the reduction of nitrogen oxides, *J. Catal.* 235 (2005) 201–208.
- [36] R.D. Zhang, N. Liu, Z.G. Lei, B.H. Chen, Selective transformation of various nitrogen-containing exhaust gases toward N<sub>2</sub> over zeolite catalysts, *Chem. Rev.* 116 (2016) 3658–3721.
- [37] Y. Xin, Q. Li, Z. Zhang, Zeolitic materials for DeNOx selective catalytic reduction, *ChemCatChem* 10 (2018) 29–41.
- [38] C. Paolucci, I. Khurana, A.A. Parekh, S. Li, A.J. Shih, H. Li, J.R.D. Iorio, J.D. Albarraín-Caballero, A. Yezersets, J.T. Miller, W.N. Delgass, F.H. Ribeiro, W.F. Schneider, R. Gounder, Dynamic multinuclear sites formed by mobilized copper ions in NOx selective catalytic reduction, *Science* 357 (2017) 898–903, <http://dx.doi.org/10.1126/science.aan5630>.
- [39] J. Kim, S.J. Cho, D.H. Kim, Facile synthesis of KFI-type zeolite and its application to selective catalytic reduction of NOx with NH<sub>3</sub>, *ACS Catal.* 7 (2017) 6070–6081.
- [40] D. Jo, T. Ryu, G.T. Park, P.S. Kim, C.H. Kim, I.-S. Nam, S.B. Hong, Synthesis of high-Silica LTA and UFI zeolites and NH<sub>3</sub>-SCR performance of their copper-exchanged form, *ACS Catal.* 6 (2016) 2443–2447.
- [41] W. Epling, L. Campbell, A. Yezersets, N. Currier, J. Parksii, Overview of the fundamental reactions and degradation mechanisms of NOx storage/reduction catalysts, *Catal. Rev.* 46 (2004) 163–245.
- [42] D.H. Kim, K. Mudiyanselage, J. Szanyi, J.H. Kwak, H. Zhu, C.H.F. Peden, Effect of K loadings on nitrate formation/decomposition and on NOx storage performance of K-based NOx storage-reduction catalysts, *Appl. Catal. B* 142–143 (2013) 472–478.
- [43] L. Jaeha, Y.S. Ryoo, S.J. Cho, H. Lee, C.H. Kim, D.H. Kim, Investigation of the active sites and optimum Pd/Al of Pd/ZSM-5 passive NO adsorbers for the cold-start application: evidence of isolated-Pd species obtained after a high-temperature thermal treatment, *Appl. Catal. B* 226 (2018) 71–82.
- [44] L. Castoldi, R. Matarrese, S. Morandi, L. Righini, L. Lietti, New insights on the adsorption, thermal decomposition and reduction of NOx, over Pt- and Ba-based catalysts, *Appl. Catal. B* 224 (2018) 249–263.
- [45] Q. Gu, J. Long, L. Fan, L. Chen, L. Zhao, H. Lin, X. Wang, Single-site Sn-grafted Ru/TiO<sub>2</sub> photocatalysts for biomass reforming: synergistic effect of dual co-catalysts and molecular mechanism, *J. Catal.* 303 (2013) 141–155.
- [46] L. Calzada, S. Collins, C. Han, V. Ortalan, R. Zanella, Synergistic effect of bimetallic Au-Ru/TiO<sub>2</sub> catalysts for complete oxidation of methanol, *Appl. Catal. B* 207 (2017) 79–92.
- [47] H. Pan, Y. Guo, Y. Jian, C. He, Synergistic effect of non-thermal plasma on NOx reduction by CH<sub>4</sub> over an In/H-BEA catalyst at low temperatures, *Energy Fuel* 29 (2015) 5282–5289.
- [48] L. Li, L. Qu, J. Cheng, J. Li, Z. Hao, Oxidation of nitric oxide to nitrogen dioxide over Ru catalysts, *Appl. Catal. B* 88 (2009) 224–231.
- [49] E.E. Miró, L. Gutierrez, J.M.R. López, F.G. Requejo, Perturbed angular correlation characterization of indium species on In/H-ZSM5 catalysts, *J. Catal.* 188 (1999) 375–384.
- [50] M.C. Campa, D. Pietrogiacomi, M. Occhizzi, The simultaneous selective catalytic reduction of N<sub>2</sub>O and NOx with CH<sub>4</sub> on Co- and Ni-exchanged mordenite, *Appl. Catal. B* 168–169 (2015) 293–302.
- [51] L. Li, J. Yu, Z. Hao, Z. Xu, Novel Ru-Mg-Al-O catalyst derived from hydrotalcite-like compound for NO storage/decomposition/reduction, *J. Phys. Chem. C* 111 (2007) 10552–10559.
- [52] L. Qu, J. Li, Z. Hao, L. Li, Catalytic oxidation of nitric oxide to nitrogen dioxide on Ru-FAU, *Catal. Lett.* 131 (2009) 656–662.
- [53] Z. Li, M. Flytzani-Stephanopoulos, Selective catalytic reduction of nitric oxide by methane over cerium and silver ion-exchanged ZSM-5 zeolites, *Appl. Catal. A* 165 (1997) 15–34.
- [54] M. Colombo, I. Nova, E. Tronconi, NO<sub>x</sub> adsorption on Fe- and Cu-zeolite catalysts: the effect of the catalyst red-ox state, *Appl. Catal. B* 111–112 (2012) 433–444.
- [55] G. Zhou, T. Luo, R.J. Gorte, An investigation of NOx storage on Pt-Ba-O-Al<sub>2</sub>O<sub>3</sub>, *Appl. Catal. B* 64 (2006) 88–95.
- [56] G. Liu, P.X. Gao, A review of NOx storage/reduction catalysts: mechanism, materials and degradation studies, *Catal. Sci. Technol.* 1 (2011) 552–568.
- [57] M. Wallin, C.J. Karlsson, M. Skoglundh, A. Palmqvist, Selective catalytic reduction of NOx with NH<sub>3</sub> over zeolite H-ZSM-5: influence of transient ammonia supply, *J. Catal.* 218 (2003) 354–364.
- [58] S.A. Bates, W.N. Delgass, F.H. Ribeiro, J.T. Miller, R. Gounder, Methods for NH<sub>3</sub> titration of Brønsted acid sites in Cu-zeolites that catalyze the selective catalytic reduction of NOx with NH<sub>3</sub>, *J. Catal.* 312 (2014) 26–36.
- [59] A. Simperler, R.G. Bell, M.D. Foster, A.E. Gray, D.W. Lewis, M.W. Anderson, Probing the acid strength of bronsted acidic zeolites with acetonitrile: an atomistic and quantum chemical study, *J. Phys. Chem. B* 108 (2004) 7142–7151.
- [60] W. Dai, X. Sun, B. Tang, G. Wu, L. Li, N. Guan, M. Hunger, Verifying the mechanism of the ethene-to-propene conversion on zeolite H-SSZ-13, *J. Catal.* 314 (2014) 10–20.
- [61] K. Hadjiivanov, Identification of neutral and charged NxOy surface species by IR spectroscopy, *Catal. Rev. Sci. Eng.* 42 (2000) 71–144.